Superconducting-nanowire-single-photon-detectors in a magnetic field

Bob Rengelink

March 1, 2013

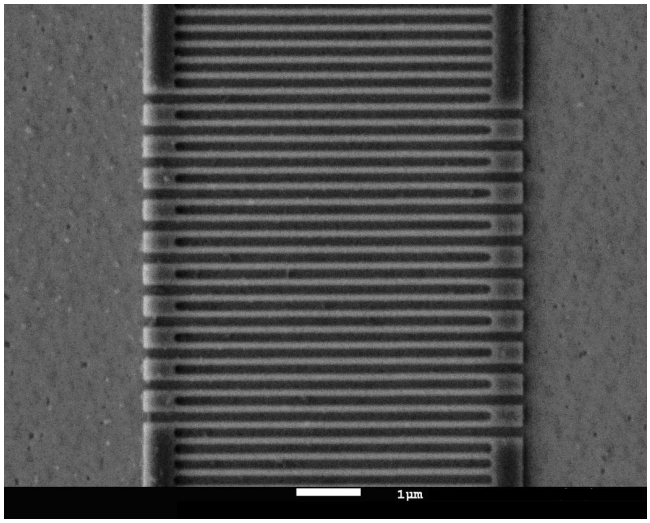

Master Thesis
Supervised by: Jelmer Renema and Martin van Exter
Quantum optics group
Leiden University

Abstract

Current-voltage and count rate measurements were performed on a NbN Superconducting-single-photon-detector in a magnetic field perpendicular to the meander plane. The critical current dependence on the magnetic field was found to be asymmetric with respect to the direction of the magnetic field, indicating an intrinsic asymmetry in the detector. Both the dark count rate and the photon detection rate were found to display effects that cannot be explained in terms of the hotspot model.

Contents

1 Introduction

In recent years, superconducting nanowire single photon detectors (SSPDs) have become a promising new technology for fast single photon detection in the infrared. They typically consist of a very thin (≈ 4 nm) superconducting nanowire in the form of a meander pattern and were first developed in 2001 [1]. Although the physics involved in the detection process is not yet completely understood, SSPDs already outperform conventional detectors in most of the parameters considered important for a photon detector.

The current state of the art in terms of performance is set by electronics limited timing jitter (tens of picoseconds), count rates of up to tens of MHz, detection efficiencies of up to 93% [2] at a wavelength 1550 nm, and a dark count rate of the order of a few per second. Especially because they combine all of these features in the same device and cover a broad wavelength spectrum, SSPDs compare favorably to alternatives such as InGaAs avalanche photodiodes or transition edge sensors [3].

Their unparalleled performance makes SSPDs a very useful device in many scientific fields, such as quantum optics [4][5][6] , quantum cryptography [7] and astronomy [8]. A number of technological applications such as long distance classical communication [9] and LIDAR [10] could also benefit from these detectors.

Although SSPDs were invented over ten years ago, the physics involved is not yet comprehensively understood. The detection model of the device, the so-called hotspot model, is not yet able to quantitatively explain important features of the device, such as the non-linear photon number response and the exact energy scaling. Another important issue is that the origin of dark counts is at present still unknown.

In order to try to gain more understanding of what happens in the detection process, we measured the characteristics of the detector when a magnetic field was applied to it. Because SSPDs are superconducting devices, we expect them to interact strongly with a magnetic field, possibly changing the behavior of the detector dramatically. This magnetic field dependence has only recently become an active subject of research [11].

The general outline of this thesis is straightforward: First, section 2 reviews the hotspot model and a bit of superconductivity theory. It will also treat some of the subtleties involved in the electronic operation of the device. Then section 3 will explain the experimental set-up for both DC and AC measurements. Finally, section 4 will discuss the results that were obtained.

2 Theory

2.1 Basic superconductivity theory

For most superconducting materials, a description in terms of a combination of the microscopic Bardeen-Cooper-Schrieffer (BCS) theory and the more phenomenological Ginzburg-Landau (GL) theory is sufficient. A good introduction to the subject is the book by Micheal Tinkham [12]. For an in-depth treatment of BCS theory "The classical condensates" by Jan Zaanen is an excellent resource [13]. It should be noted, however, that superconductivity is a large and active area of research, and consequentially a large selection of literature is available to the interested reader. Rather than giving a complete treatment, this section will only give a brief description of the concepts essential to understanding SSPDs.

Critical current, temperature and magnetic field

Superconducting materials have two defining properties which are tightly linked: 1) They conduct electricity without dissipation and 2) they expel magnetic field from their interior, a phenomenon known as the Meissner effect. In a nutshell, BCS theory states that this behavior is caused by the fact that the superconducting condensate is made up of bound states of two electrons known as Cooper pairs. The supercurrent shows up as a first-order perturbation to the order parameter of this condensate that is well defined in the limit of small currents(section 6.1 of ref. [13]). The Meissner effect arises because the order parameter also defines the form of the vector potential inside of the superconductor. The most important microscopic parameter characterizing the superconducting state is the binding energy of the Cooper pairs, known as the superconducting energy gap.

However, the supercurrent cannot be increased indefinitely as the current has the effect of lowering the energy gap, up to the point that this energy becomes zero and the device transitions into the normal state. The current at which this effect occurs is known as the depairing current(p125 of ref. [12]). Both temperature and an applied magnetic field will also lower or even remove the energy gap. This means that a two-dimensional critical surface is spanned by current, magnetic field, and temperature which separates the superconducting state from the normal state.

In any practical device, the superconductivity will fail before this theoretical maximal current is reached. This is caused by material defects and the spatial inhomogeneity of the current density. For this reason it is important to keep in mind that a measurement of the highest possible supercurrent in a device is not a direct measurement of the depairing current. The maximal measured current at which the device is still superconducting will be referred to as the (experimental) critical current of the device.

Vortices

According to GL theory, the Meissner effect is characterized by the ratio of two microscopic parameters: The magnetic penetration depth λ_{eff}, which sets the distance over which the magnetic field penetration into the material decays, and the coherence length ξ, which sets the distance over which the superconducting state decays into the normal state. This allows us to distinguish two types of superconductors, Type I and Type II, which display very different macroscopic behavior. A quantitative criterion can be formulated as

follows:(p135 of ref. [12])

$$\frac{\xi}{\sqrt{2}\lambda_{eff}} \quad \begin{cases} < 1 & \text{Type I} \\ > 1 & \text{Type II} \end{cases} \tag{1}$$

The difference between these two types is that type I superconductors do not allow flux to penetrate the bulk of the material, while type II superconductors allow some magnetic flux to penetrate the material in the form of an Abrikosov vortex(p143 of ref. [12]). A vortex is an elementary unit of magnetic flux surrounded by a screening current. Vortices may appear either in response to an applied magnetic field or as vortex-antivortex pairs which appear as thermal fluctuations of the superconducting state. Because thin films of NbN are type II superconductors we must take these vortex states into account.

Kinetic inductance

A highly conductive material is also an inductive material. The reason for this is that a current is also a flow of momentum because it carries not only charge, but also mass. In resistive materials, the inertia of this momentum flow is dissipated quickly by scattering but in high conductivity materials, which are in the limit of ballistic transport, the momentum flow may persist over long distances. A change in the current is therefore counteracted by its mechanical inertia which appears as a kinetic inductance. The kinetic inductance of an SSPD device can be significant and plays a large role in its operation, as explained in section 2.3.

2.2 The hotspot model of SSPDs

In order to explain the photo-response of SSPDs, a model was proposed by Goltsman et al.[1], which is known as the hotspot model. While it is quite general and takes into account only basic superconductor physics, it is able to explain some qualitative features of the SSPD detection process and it remains the most important model available in the literature.

An illustration of the detection process is shown in Fig. 1. The energy of a photon is typically much higher than the superconducting bandgap (about 3 meV, while 850 nm photons carry about 1.5 eV). Therefore, when the detector absorbs a photon, it will break a cooper pair and excite a highly energetic quasi-particle. After this initial excitation, the quasi-particle cascades into more quasi-particles until a small hotspot on the material has transitioned into the normal state. This local hotspot is no longer superconducting and the current is redirected around it. The initial formation of this hotspot depends on material properties and local bias current because both influence the energy gap, but it does not depend on the geometry of the wire. The formation of a hotspot is a necessary but not sufficient condition for a detection event to take place.

Following the formation of a hotspot, the high energy quasi-particles will diffuse into the superconducting material around it. This causes the normal domain to grow but some of the initial energy is also lost to the substrate in the form of heat. In the absence of bias current the normal region would slowly cool down and become superconducting again. When a significant bias current is applied however, the conventional hotspot model predicts that the current density redirected around the hotspot may be pushed over the critical current causing a slab of material to become normal. By Joule heating this resistive

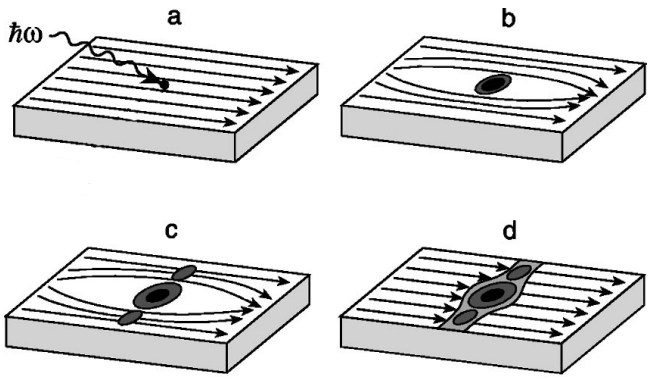

Figure 1: *Schematic picture of photon detection in the hotspot model. The device starts out biased at some temperature slightly lower than the critical current. After a while a photon is absorbed. a) The absorbed photon breaks a cooper pair and creates a highly excited quasi-particle. Immediately this quasi-particle decays and excites more quasi-particles, forming a local hotspot. b) The quasi-particles diffuse out of the hotspot creating a small normal region that redirects the supercurrent. c) the current density next to the hotspot exceeds the critical current and also becomes normal. d) A resistive slab forms and conducts a dissipative current. Joule heating causes this normal region to grow as long as a current exists. Taken from [1].*

slab will grow until a significant portion of the device has become normal. This causes a major increase in resistance which is easily detectable with a simple electronic circuit.

There are two stages of the hotspot model where important objections may be raised. The first one is the diffusion of quasi-particles out of the hotspot. According to the conventional hotspot model, this creates a local normal domain which redirects the supercurrent. It is unclear however, if a local hotspot is actually formed or whether the diffusing quasi-particles simply decrease the density of charge carriers forcing the remaining carriers to accelerate which is equivalent to locally lowering the gap rather than surpressing it completely. While this does not affect the qualitative aspects of the model for single photon detection, it does influence the expected energy dependence of the detection efficiency [14].

The second important objection is regarding the way the current density is redirected and finally pushed over its critical value. There are a lot of superconductivity effects that may play a role here, such as the formation of phase slip centers [15], interaction with vortices [16] and the Johnson effect [12]. It is also very dependent on the local geometry of the wire and of the normal domain formed by the diffusing quasi-particles. In summary, the hotspot model sketches a simple and intuitive picture, but it leaves many important questions unanswered and has not yet been conclusively confirmed.

2.3 Thermo-electric switching

The electronic measurement of a detection event can be modeled very well by a thermo-electric model by Kerman [17]. In this thermo-electronic model, the detector is modeled as a simple electronic device consisting of an inductor in series with a variable resistor, as shown in Fig. 2a. For the sake of convenience we will use a simplified detection model that assumes instantaneous switching of the detector's resistance. This model is unphysical, but provided that the timescale involved in the switching is small compared to the timescales described below, it accurately predicts the detector's pulse shape as shown in Fig. 2b.

As shown in Fig. 2a, if the device is superconducting all current will flow through the detector and there is no current going through the load R_L which is typically the input impedance of an amplifier (50 Ω). When a photon is detected the model assumes that the resistance of the detector increases on a timescale much shorter than all other timescales of the system. This is modeled simply by setting the resistance of the detector to the normal state resistance (≈500 kΩ) instantaneously. The current will now be redirected through the load resistance instead. The time constant over which this happens is set by:

$$\tau_{rise} = \frac{L}{R_L + R_n} \tag{2}$$

This time constant is also a minimum that can be set to the rise time of the detector. The kinetic inductance of an NbN nanowire is known to scale linearly with normal state resistance at room temperature [18]. This dependence allows us to estimate the inductance of our detector to be about 100 nH, indicating a minimum rise time smaller than 1 ps. All physics associated with the detection mechanism will increase this time, but it is still too short to be measurable with an oscilloscope.

Not long after the rise time, no more current runs through the detector, Joule heating becomes negligible, and the device cools down again. The model assumes that the resistance switches back to zero when the current through the detector falls below a certain threshold (e.g. 10^{-4} of the bias current). Now the current will be redirected to pass through the detector again. The time constant associated with this is set only by the load resistance and the device inductance:

$$\tau_{fall} = \frac{L}{R_L} \tag{3}$$

τ_{fall} is typically of the order of a few nanoseconds. This switching produces a voltage pulse over the load resistance which can be detected and has the characteristic asymmetric pulse shape shown in Fig. 2b.

Because the systems maximum count rate is set by τ_{fall}, one could think about increasing the maximum count rate by altering the circuit. The kinetic inductance cannot be easily decreased without altering the design of the detector leaving only the load resistance as a parameter. Unfortunately the following examination of the switching mechanism reveals that the device will not function properly at high load resistances.

The electronic circuit is essentially a feedback system which is made unstable on purpose. In the case that the feedback becomes stable, the undesirable phenomenon known as latching takes place. When the device latches, the cooling of the detector is not fast enough to counterbalance the joule heating caused by

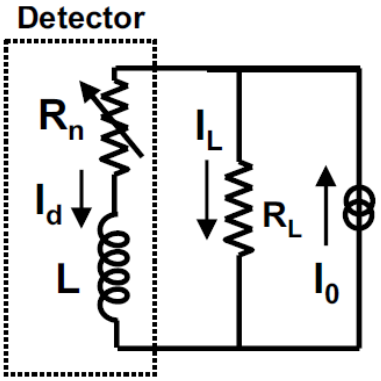

(a) *Simplified circuit diagram*

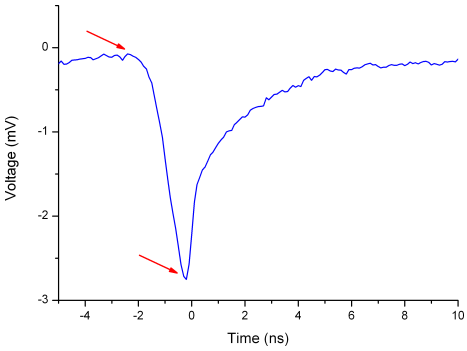

(b) *Measured voltage across R_L following a dark count*

Figure 2: *Electronic model of a SSPD. Fig. 2a: Simplified circuit diagram of an SSPD device. When the device is superconducting, there is no resistivity and R_n is set to zero in our model. After a photon or dark count event R_n switches to a value much higher than the load resistance R_L, causing the current to be redirected across R_L. The kinetic inductance discharges with time constant $\tau_{rise} = L/(R_n + R_L) \approx 1$ ps. The absence of current across R_n allows the device to cool down through the substrate and become superconducting again. The kinetic inductance charges again with a different time constant $\tau_{fall} = L/R_L \approx 2$ ns for typical values of $L = 100$ nH and $R_L = 50\Omega$. This sequence allows the detection event to be measured as a voltage peak across R_L. Fig. 2b: Average trace of 100 dark count events, measured by a single 20 dB amplifier. The first red arrow indicates the switching of the detector into the normal state. The second red arrow indicates the point where the detector switches back to the superconducting state. Circuit diagram taken from [17].*

the returning bias current and a stable normal domain remains on the detector. For this reason, the count rate of the detector is ultimately limited by its kinetic inductance and by the thermal contact to the substrate.

The transition from stable to unstable feedback can be seen in the device IV curve. Fig. 3 shows three different regimes on a typical IV curve that show this effect. Up to the voltage at which the critical current is reached, the device is superconducting. The regime where the detector is taken a little bit over the critical current is called the relaxation oscillation regime [19], in this regime the detector oscillates between fully superconducting and partially normal as neither state is stable. If the voltage is increased further, a small normal strip across the wire becomes stable and grows in response to the applied voltage. This regime is known as the hotspot plateau.

2.4 Dark counts in SSPDs

Even in the absence of light and interferences, SSPDs still produce a small, but non-negligible, amount of dark counts. The origin of these dark counts is not yet fully understood but they are most likely a thermally activated process. Several models have been proposed for this, mostly involving vortex dynamics or

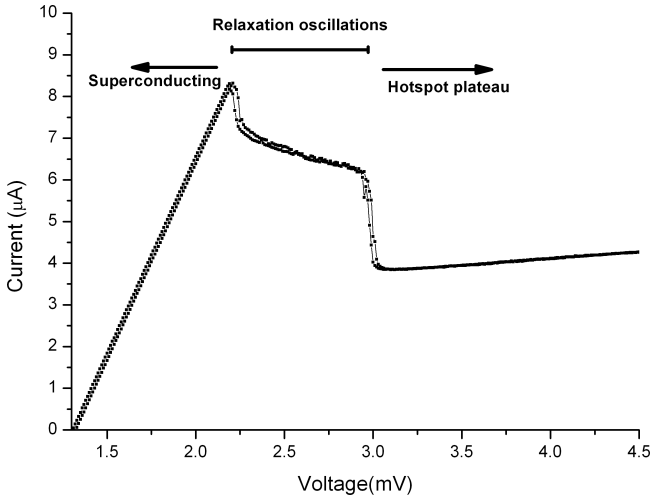

Figure 3: *Typical meander-type SSPD IV curve. Three different regimes can be identified which are indicated in the figure. At low bias voltage the device is superconducting until it reaches its critical current. At this point the detector enters the relaxation oscillation regime where there is no stable current configuration and the device oscillates between a superconducting and a partially normal state. Finally, when the voltage is increased to the point where a hotspot can be formed that is stable through electrothermal feedback, the system enters a regime known as the hotspot plateau.*

phase-slip centers. [16] An important feature of thermally activated dark counts is temperature scaling:

$$R_{DC} \propto \exp -\frac{E_a}{k_b T} \tag{4}$$

Where R_{DC} is the dark count rate, and E_a is the activation energy of the process. Most models lead to an approximately linear scaling of the energy barrier E_a with bias current, leading to an exponential scaling with bias current as well as (inverse) temperature.

3 Experimental setup

3.1 Experimental set up

All measurements were performed on a meander type detector nominally identical to the one shown in Fig. 4. The detector was fabricated by A. Gaggero, F. Mattioli and R. Gleoni at the CNR-IFN in Rome and consists of a 4 nm thick NbN nanowire on top of a GaAs substrate. The meander pattern has a total of 21 wires of 100 nm width and 150 nm spacing constituting a total active area of 5x5 μm^2) with a 40 % fill factor. In relation to fundamental superconducting length scales this means that the magnetic penetration depth, which is of the order of a few μm at typical operating temperatures, is large compared to the width of the wire, while the coherence length, which is a few nm, is small. The wire is wider at the corners to minimize current crowding. At room temperature the total resistance of the detector is about 650 kΩ.

Fig. 5 shows the experimental set-up used in most of the experiments. The detector was cooled in a Quantum Design PPMS-6000 cryostat. The same device was also fitted with a superconducting magnet able to produce bipolar magnetic fields up to 9 T. A Yokogawa GS-210 DC voltage source was used to voltage bias the detector. A mini-circuits bias-tee was used to separate the DC bias voltage from the AC signal produced by the detector. The signal was amplified and then detected. This was done either by a Lecroy wavepro 7300A oscilloscope capable of measuring up to 6 GHz signals, or an Agilent pulse-counter. A more detailed view of the electronics involved in the experiment is shown schematically in Fig. 6. The DC arm in front of the bias-tee contains a 100 Ω resistor with an Agilent voltmeter in parallel to monitor the bias current. Amplification was done by three 13 dB mini-circuits AC amplifiers.

The detector is very sensitive to AC interference. As a rule of thumb, an interfering current signal will lower the critical current by an amount comparable to its amplitude [20]. For this reason a very stable voltage source is required and care must be taken to limit electronic interference as much as possible. Because of the low voltages involved, another electronic problem is caused by multiple grounds that don't have the same potential. This was solved by plugging all of the electronics in the same power socket and adding a few grounding cables to the set-up. Even with perfect grounding a small voltage offset of about 1.3 mV remained. Most likely this was a thermoelectric voltage resulting from a different temperature gradient over the inside and the outside of the wire [21]. Because the voltage showed up as a DC offset only it could easily be compensated with the voltage source.

In order to measure the optical response of the detector, a 850 nm Thorlabs diode laser was coupled into a single-mode optical fiber. This fiber was led into the cryostat and finally coupled to a lens in order to make a parallel beam (cross section $\approx 1\ cm^2$) that illuminates the detector. The spot will always be much larger than the detector and consequently the current set-up will only allow a relative measurement of the detection efficiency.

3.2 IV characteristic measurements

During DC measurements, the amplifiers were replaced by a 50 Ω terminator in order to reduce high frequency noise going into the detector. Because of the

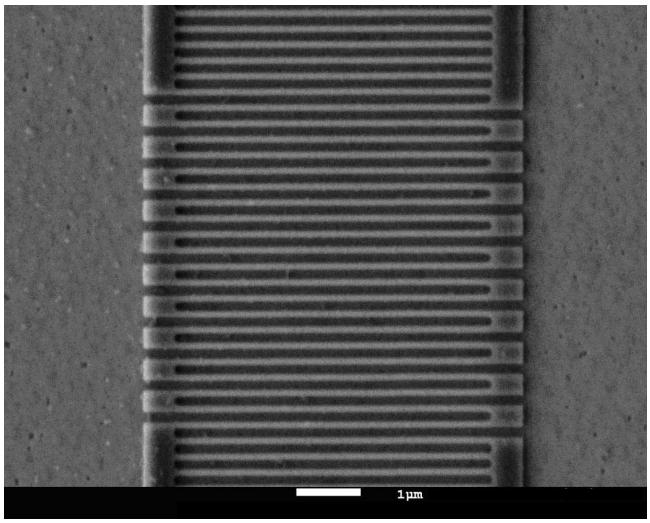

Figure 4: *SEM picture of a meander-type detector nominally identical to the one used in our experiments. The picture is made by D. Sahin, TU/e. This detector was not the one used in the experiments, but it was fabricated on the same sample.*

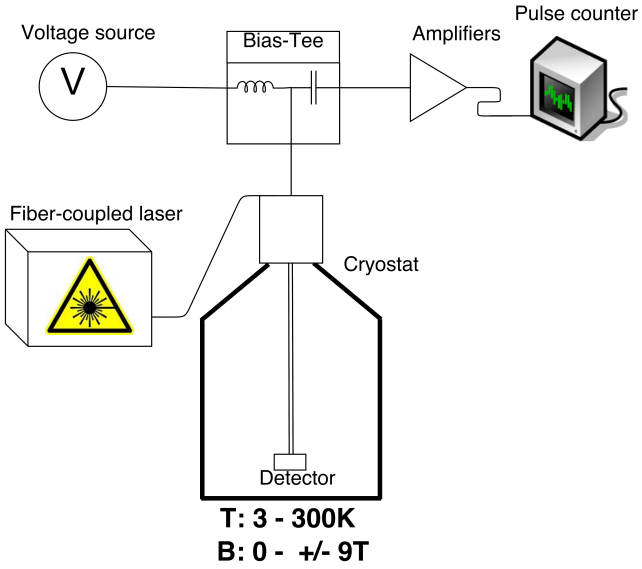

Figure 5: *Simplified diagram of the set-up. The detector is biased with a DC voltage source. The AC response of the device is separated by a bias-tee, amplified and counted with an electronic pulse counter. A fiber-coupled laser is used to shine light on the device. The cryostat allows detailed control over both temperature and magnetic field.*

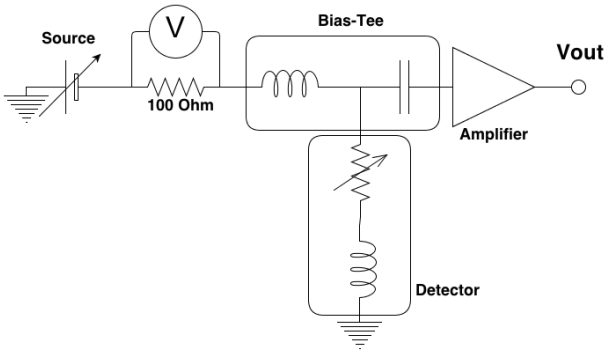

Figure 6: *Circuit diagram of the electronics. A voltage is applied to both a 100 Ω resistor and the detector, causing a current to flow. The bias-tee separates the DC circuit from the AC circuit, and finally the signal from the detector is amplified and detected.*

high degree of non-linearity in the IV characteristic of the detector, a series resistance that is too large will allow multiple (I,V) solutions to the non-linear system created by the detector and the resistance. [19] This can potentially change the measured IV characteristic of the total system and obscure the relaxation oscillation regime. The 100 Ω series resistance was low enough to prevent this from happening, but high enough to allow a reasonably accurate current measurement.

3.3 Dark counts measurements

In order to measure count rates, the amplified detector output was measured by a pulse counter with the trigger level set to an appropriate value. This value was determined by measuring the pulse height with an oscilloscope. The trigger level was then chosen to be somewhere in between the noise peaks and the average pulse height. The total number of counts was measured every second for at least one full minute. In post processing the average and standard deviation of the number of counts per second was calculated. Count rates that were several standard deviations away from the average were assumed to be caused by electronic interference and were ignored in a second and final calculation of the average number of counts per second.

3.4 Optical measurements

Light count measurements were performed in much the same way as dark counts measurements with the addition of a 850 nm laser. The laser output power was checked for linearity and was found to deliver about a milliwatt of output power at the output of the fiber. This power was kept at the same level for all measurements presented in this report.

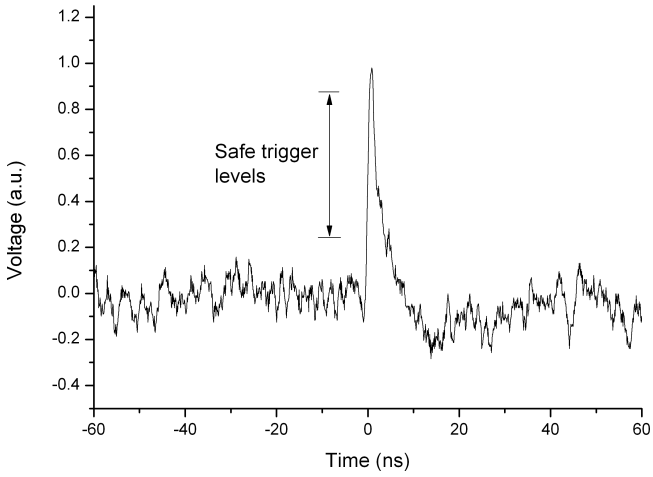

Figure 7: *Dark count measured with an oscilloscope. This measurement was typically taken to estimate the required trigger level for the pulse counter. The trigger level has to be significantly higher than the noise peaks so as not to detect noise peaks as count events, but not so high that real detection events are not registered. The acceptable range of trigger levels is indicated in the figure.*

4 Results

4.1 Dependence of the critical current on the magnetic field

IV curves were taken at a constant temperature of 3 K for different magnetic field strengths. The field was oriented perpendicular to the film for all experiments. From these, the critical current was determined by taking the highest current in a small voltage range around zero current, as indicated in Fig. 8. This range was chosen to be small compared to the voltage at which the device starts to transition into the normal state, such that the peak of the critical current was always the maximum current within this range. For high fields and temperatures the critical current no longer appears as a clear peak and the device instead gradually transits from superconducting behavior into normal resistive behavior. In this case the peak criterium is no longer valid and a resistivity criterium should be used instead [20]. For fields of up to 1 T this was not necessary.

Fig. 9 shows the measured critical current as a function of the magnetic field. We find that in a magnetic field the observed critical current can be either higher or lower depending on bias current polarity. We even found that a relatively weak magnetic field of several tens of mT can increase the critical current by about 8%. A typical IV curve is shown in Fig. 10a, where a magnetic field in two directions shows a nearly perfect symmetry upon reversing the polarity of both the current and the field simultaneously. Further results in Fig. 10b show that the effect of changing the field direction and switching the current direction are entirely equivalent. Because of this equivalence we conclude that the observed asymmetry is an effect that is inherent to the device and not an experimental artifact.

The nominal structure of the detector is symmetric both with respect to the direction of the current and the polarity of a perpendicular magnetic field individually. The observed asymmetry can therefore only be explained by imperfections of one form or another within the device. A similar effect was found recently in TaN meander detectors [11] and was interpreted to be the result of imperfections in the corners of the meander. While attributing the imperfections to the bends in the meander is plausible and intuitively appealing it is not the only possible explanation as any localized imperfection in the superconducting wire that is not symmetric with respect to the lateral direction of the wire can explain the observed asymmetry.

4.2 A broader look at the IV characteristics

We also probed the IV characteristic of the device at larger voltage scales. Results from these measurements are shown in Fig. 11. The IV characteristic shows steps known as fringes[1] which result from device geometry [22]. The explanation is as follows: as the voltage across the device is increased one wire will first transition into the normal state, reducing the total current passing through the device. If the voltage is increased further a second wire will transition into the normal state. This process repeats until the entire device has become normal.

[1] Not in any way related to optical interference fringes.

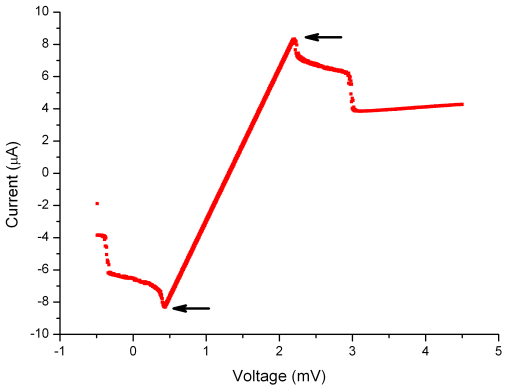

Figure 8: *A typical IV curve at 3 Kelvin and no magnetic field. Critical currents are indicated by the arrows. In most cases the critical currents were simply the minimum and maximum values of the current within the range of applied voltages.*

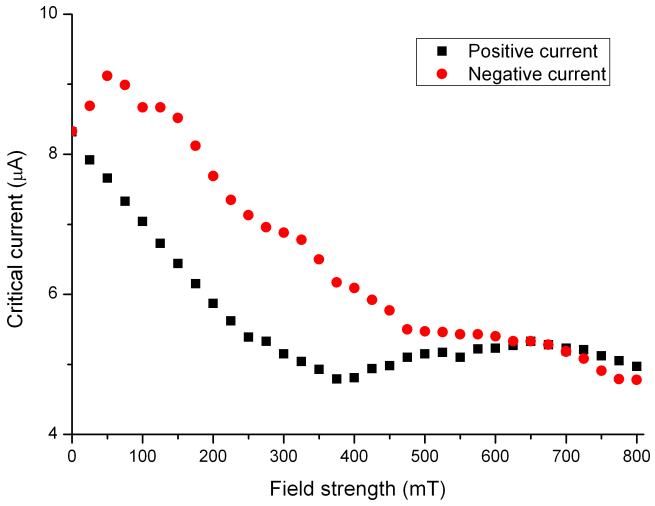

Figure 9: *Observed critical current as a function of magnetic field. Bias current was applied to the device both with positive and negative polarity. The plot shows an asymmetry between biasing with a positive and a negative current. This result points to an intrinsic asymmetry of the detector.*

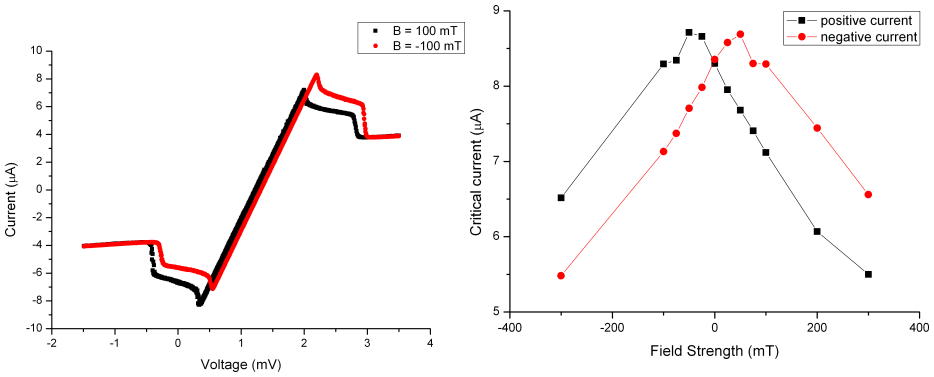

(a) *IV curves in a ±100 mT magnetic field* (b) *Detail of the observed critical current as a function of magnetic field*

Figure 10: *(10a): Two typical IV curves taken with the detector in a ± 100 mT magnetic field. At both times the field was perpendicular to the film but in opposite direction. The IV curves are almost completely symmetric upon switching the sign of the current. (10b): The asymmetry of the critical current dependence about the magnetic field strength axis. The plot shows that switching the sign of the current and of the field is equivalent. Both results indicate that the asymmetry observed in the IV curve are inherent to the detector.*

The resistance of each of the wires should be equal to a fraction of exactly $1/n$ of the total normal state resistance, where n is equal to the total number wires.

We found that the differential resistance increased by about $45k\Omega$ at each step by fitting our data with a different straight line at each step. After correcting for our offset voltage these linear fits also passed through the origin, indicating linear electronic behavior. The value of the resistance found in this way should correspond to the resistance of a single wire. The device has 21 wires and a normal state resistance of about 650 $k\Omega$ at room temperature. The normal state resistance of a different device on the same sample was measured to be 37% higher at cryogenic temperatures compared to room temperature [21]. Using these numbers we estimate the normal state resistance of a single wire to be about $1.37 * 650/21 \approx 42$ $k\Omega$.

When a magnetic field is applied, it has the effect of making the steps less pronounced as shown in Fig. 11b. A possible explanation for this is that the magnetic field pushes the current to one side of the wire. This leads to a change in position where the normal domain nucleates and the way in which it then starts to grow. At high fields the current density is highly concentrated at the edge of the wire and a gradual increase in resistance along the edge of the entire meander becomes more likely.

At lower voltages, a very similar type of step behavior is found, as shown in Fig. 12. As with the fringes we observe that the steps smooth out in a magnetic field. The resistance now increases in steps of 4 $k\Omega$ but the value of this number can not be explained by simple geometry as is the case with fringes. This step behavior was previously documented for our detector [21] and has also been observed in straight thin wire [23]. This seems to indicate that a single wire becomes normal in discrete steps but as of yet no plausible mechanism has been proposed for this behavior.

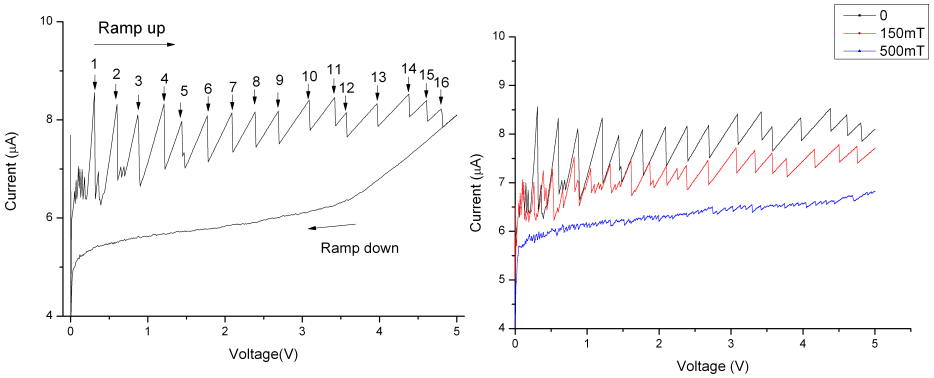

(a) *IV characteristic of the detector at larger Voltages and no field.*

(b) *IV characteristic at larger voltages and different magnetic fields*

Figure 11: *(11a): IV curve at larger voltages. The voltage was ramped up and down producing a number of "fringes", indicated by the numbered arrows, during the ramp up and hysteretic behavior during the ramp down. The fringes are caused by the wires of the device becoming normal one at a time. The increased steepness of the curve corresponds to an increase in resistance of about* $45k\Omega$ *per step. The hysteretic ramp down was not shown in subsequent plots for clarity. Figure 11b shows the same measurement at various field strengths. The fringes disappear at higher fields.*

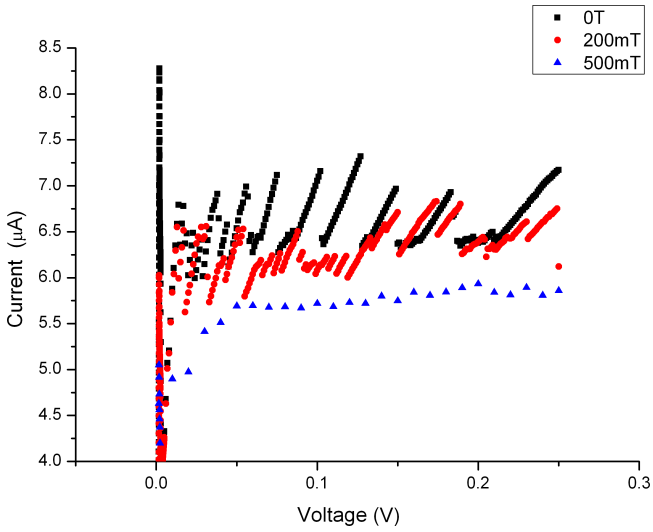

Figure 12: *IV curve in an intermediate voltage range. A step behavior very similar to the fringes is found. Without any field the increased steepness of the curve corresponds to an increase in resistance of about* $4k\Omega$ *per step. The precise origin of the steps is at present unknown. The steps smooth out at higher field strengths*

4.3 Dark counts in a magnetic field

Dark counts were measured as a function of bias current at magnetic field strengths ranging from -300 to 300 mT. Results of these measurements are shown in Fig. 13 and Fig. 14. The former shows the behavior over the entire range of magnetic fields while the latter gives a more detailed look at low magnetic fields.

All results show an exponential increase in dark counts as a function of bias current. Several features of these exponential increases change in a magnetic field. The most obvious change is that the maximal count rate point of the curve reflects the change in critical current in response to the magnetic field. A more subtle effect is that the count rate curves with an applied field of up to -150 mT in one direction, and up to 50 mT in the other direction, have a lower count rate than at zero field for most data points on the curve.

Fig. 14 shows the count rate curve becoming progressively lower as the field is increased. It also shows an apparent qualitative change in behavior of the dark count rate. At magnetic fields lower than 30 mT, a multi-exponential increase in dark counts can be observed. For all other field strengths the increase in dark counts was approximately single exponential.

By linearly interpolating the logarithm of the count rate as a function of bias current, the count rate as a function of magnetic field could be determined at a fixed bias current. The result for a bias current of 6.5 μA, shown in Fig. 15, shows a minimum in the count rate for both polarities of the field, indicating that a magnetic field of about 50 to 100 mT reduces dark count rates by two to three orders of magnitude compared to the count rate at zero field.

The asymmetry with respect to the direction of the magnetic field, shown in Fig. 15, is most likely related to the asymmetry in the critical current shown in Fig. 9 which was argued to be a geometrical effect in section 4.1. The dramatic decrease in count rate at fields below 100 mT which occurs for both polarities of the field is not readily explained as a geometrical effect however. This decrease may have something to do with the nature of the dark counts. Because it is unclear how to separate the geometric effects from this fundamental effect we propose to continue these experiments on a different detector in the concluding section.

It should be noted that these results seem to be in conflict with measurements performed by Engel *et al.* [11], who report only a single minimum in the dark count rate at fixed current as a function of magnetic field strength. The discrepancy may be explained by the fact that the measurements performed in this study cover a much greater range of magnetic fields and that the observed asymmetry of the curves is determined by imperfections in the detector and is therefore expected to vary greatly between detectors.

4.4 Photon detection in a magnetic field

In order to characterize the detection behavior of the detector in a magnetic field, a reference measurement was performed at 3 K and no applied field. Aligning was performed by maximizing the count rate of the detector at a fixed laser output power and a fixed bias current. Fig. 16 shows the result of this reference measurement.

The maximum count rate in figure 16 is $4.3 * 10^5$ counts per second. We can

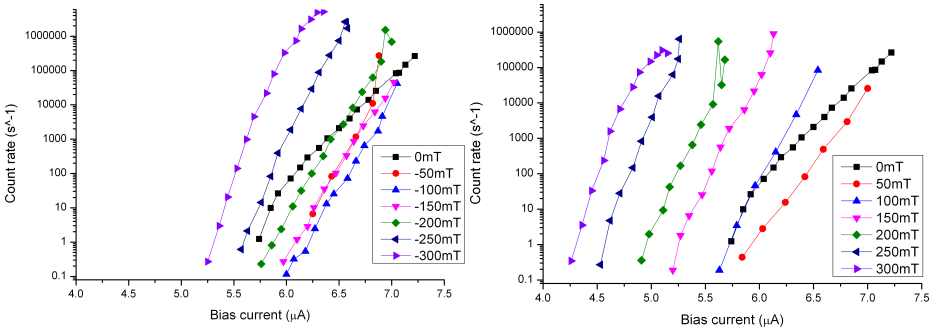

(a) *Dark counts as a function of bias current in the negative field direction*

(b) *Dark counts as a function of bias current in the positive field direction*

Figure 13: *Dark counts at a temperature of 3 K as a function of bias current at various magnetic fields perpendicular to the meander in two directions. The negative direction is the direction in which the critical current was shown to increase in section 4.1. We see that the dark count curves shift when a magnetic field is applied. Most noticable, the dark count curves at field strengths of -150 mT, -100 mT, -50 mT and 50 mT display lower count rates than the zero field curve for almost all currents.*

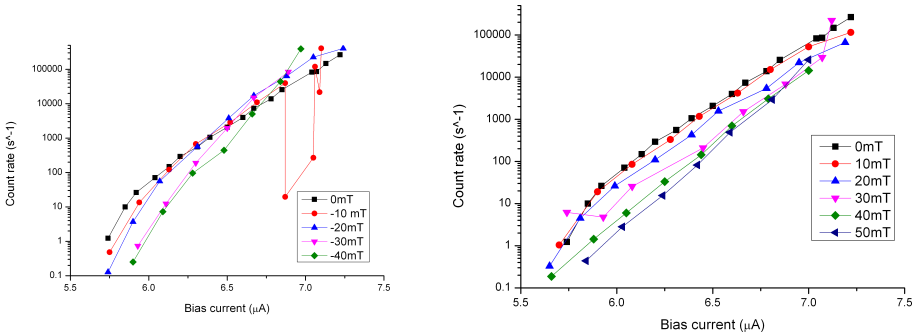

(a) *Dark counts as a function of bias current in the negative field direction*

(b) *Dark counts as a function of bias current in the positive field direction*

Figure 14: *Detail of dark counts as a function of bias current at various magnetic fields. The negative direction is the direction in which the critical current was shown to increase in section 4.1. For magnetic field strengths up to 30 mT the increase in dark counts is not strictly mono-exponential.*

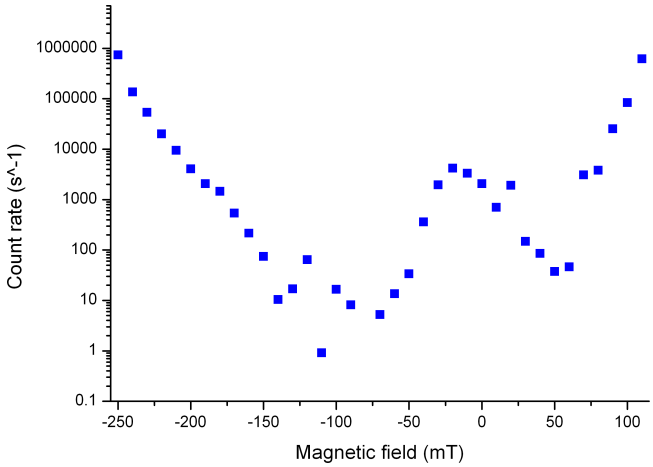

Figure 15: *Count rate as a function of magnetic field at a fixed bias current* $I_b = 6.5\ \mu A$*. A local minimum in the count rate is found for both orientations of the field.*

estimate the total number of photons incident on the detector by multiplying the total detector area ($5 * 5\ \mu\text{m}^2$) by the laser output power (≈ 1 mW), and dividing by the total spot area ($\approx 1\ \text{cm}^2$) and the energy per photon(≈ 1.45 eV). In this way it was estimated that about 10^9 photons hit the detector every second, indicating a detection efficiency of $4 * 10^{-4}$. The fabrication report on this batch of detectors [24] reports a maximum detection efficiency of 10^{-3}. It seems reasonable that we observe a somewhat lower value because we have observed a degradation of the detectors in terms of critical current and it seems likely that the detection efficiency has degraded as well.

A possible explanation for the low value of this number could be that only a small surface of the detector contributes to photon detection. A lower limit on the effective surface of the detector is found by multiplying the detection efficiency by the total area of the device: $4 * 10^{-4} * 25\mu\ \text{m}^2 = 10^4\ \text{nm}^2$. This area would correspond to a 100*100 nm^2 square on the wire, possibly a single localized constriction. This calculation does not take into account non-unity fill factor and absorption probability however, and the actual effective area is expected to be much higher.

Fig. 17 and 18 show count rate measurements performed at the same output power at different magnetic field values ranging from -500 to 300 mT and at different temperatures ranging from 2 to 5 K. The detection curves change significantly in response to a magnetic field. A straightforward effect is that some curves become dominated by dark counts for currents close to the critical current indicated by a sudden exponential increase in count rate, Fig. 17c and 17d show some clear examples. This point is shown more explicitly in section 4.5.

The detection curves at low temperature shown in Fig. 17a and 17b show an increase in count rate at a fixed bias current of up to about a factor three to four when a magnetic field is applied in either direction. This may be an indication that a magnetic field aids in the detection process. This effect is less pronounced at higher temperatures.

Another thing that can be seen in all of Fig. 17 and 18, but that is particu-

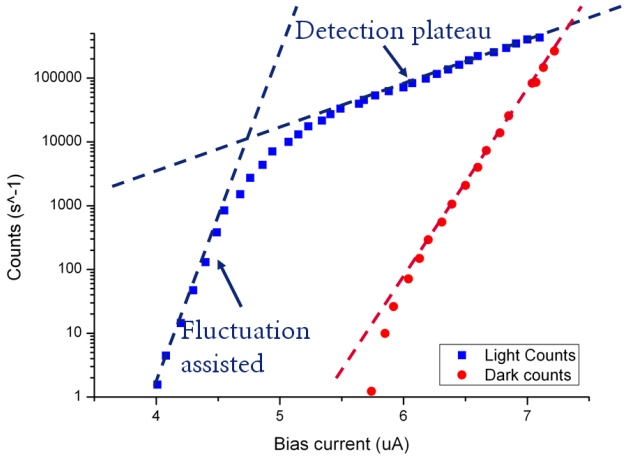

Figure 16: *Count rate with and without light on the detector and no applied magnetic field. The detection curve shows two regimes. A detection plateau, and a fluctuation assisted regime. Dark counts are shown for reference.*

larly clear in Fig. 17d and 18b, is the fact that the knee-point of the detection curve is always at a bias current of about 5 μA, regardless of critical current. This is a strong indication that the experimentally determined critical current is not what determines the shape of the detection curve. It appears that instead all of the detection curves follow a shape that varies much more slowly with magnetic field and temperature until they are cut short by the critical current.

The hotspot model predicts that a change in the shape of the detection curve is due to the decrease of the critical current. But normalizing the results for critical current is not an appropriate way of rescaling the data presented here. This is shown in Fig. 19. Instead of collapsing the data on a single curve, rescaling produces curves that are very different from one another.

Furthermore, if we compare these figures to Fig. 17a and 17b we see that the exponential tails of the detection curves, which are on top of each other when the curves aren't rescaled, are drawn away from each other. Another indication that this scaling doesn't work is the fact that a lowering of the critical current as a result of temperature does not have the same effect as lowering the critical current by applying a magnetic field.

The fact that normalizing these results for the critical current doesn't work indicates that the physics describing the changes in the light detection curves under the influence of a magnetic field can not be understood simply in terms of the hotspot model with a lower critical current. The effect of a magnetic field must therefore be considered in more detail. Unfortunately, like in the case of dark counts, it is unclear how to separate geometric effects from effects occurring in the bulk material.

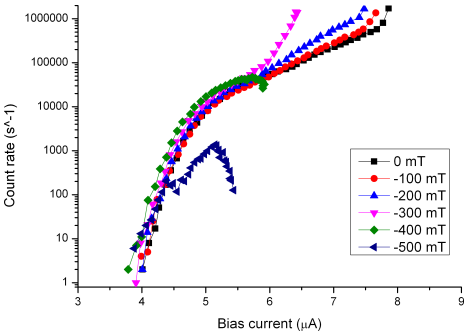

(a) *Light counts as a function of bias current in the negative field direction T = 2K*

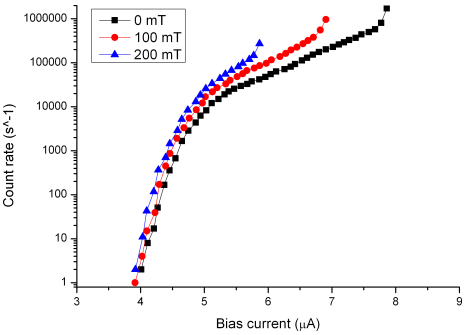

(b) *Light counts as a function of bias current in the positive field direction T = 2K*

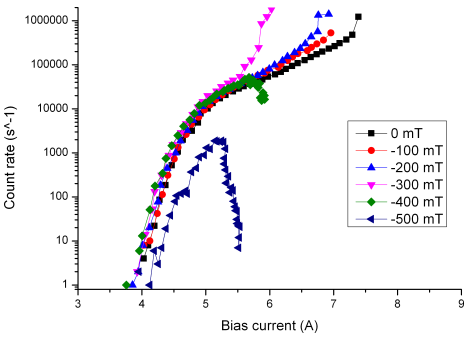

(c) *Light counts as a function of bias current in the negative field direction T = 3K*

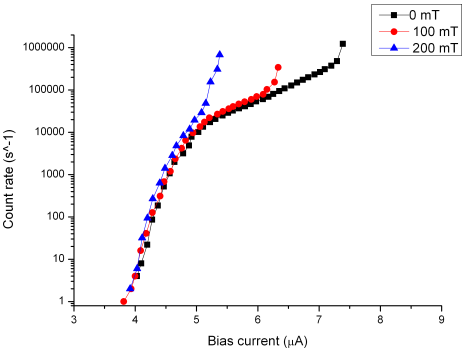

(d) *Light counts as a function of bias current in the positive field direction T = 3K*

Figure 17: *Light counts as a function of bias current in a magnetic field perpendicular to the meander in two directions and at two different temperatures. The negative direction is the direction in which the critical current was shown to increase in section 4.1.*

4.5 Magnetic-field-imposed limits on SSPDs as photon detectors

We have observed two different ways in which the detection mechanism breaks down as a result of the magnetic field such that the detector no longer functions as a photon detector. Which of these mechanisms kicks in first depends on both temperature and the direction of the magnetic field.

The most straightforward limitation is the observed increase in dark counts caused by the magnetic field. As shown in Fig. 20, the current for which dark counts become important scales more or less with critical current, whereas the detection curve does not seem to depend on the critical current directly. Typically dark count rates exceed 1000 counts per second a few tenths of μA below the critical current. At most field strengths the count rate is dominated by dark counts for currents higher than a certain current that depends on the magnetic field. At sufficiently strong magnetic fields, dark counts completely dominate

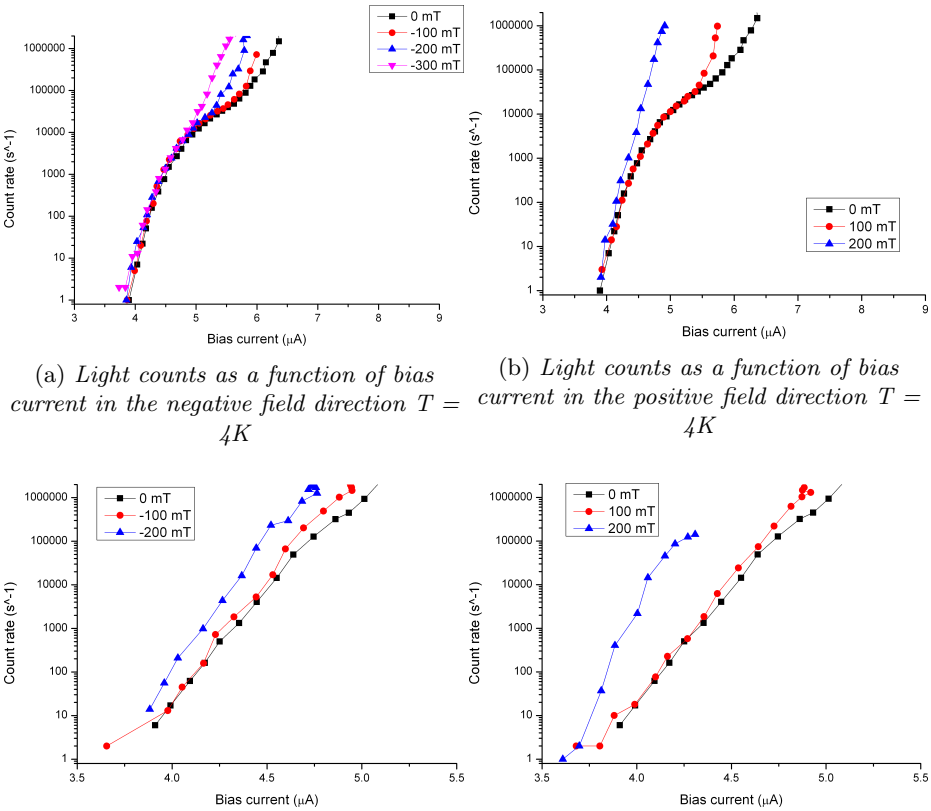

(a) *Light counts as a function of bias current in the negative field direction T = 4K*

(b) *Light counts as a function of bias current in the positive field direction T = 4K*

(c) *Light counts as a function of bias current in the negative field direction T = 5K*

(d) *Light counts as a function of bias current in the positive field direction at T = 5K*

Figure 18: *Light counts as a function of bias current in various magnetic fields and at two different temperatures. Note the different x-scale in figures 18c and 18d.*

the behavior of the detector over the entire current range.

Fig. 21 shows detection curves with the magnetic field in the negative direction. Because the critical current decreases more slowly in this direction, as shown in Fig. 9, the mechanism described above does not apply until a much higher field is applied. Instead, we observe a qualitative change in the detection curve at a magnetic field of about 400 mT. As the current nears the critical current the count rate goes down, rather than up.

The IV curve also shows a qualitative change. At 400 mT the critical current is no longer a sharp peak but instead it transitions gradually. This behavior is consistent with latching of the detector, as described section 2.3. Vortices penetrating the material in response to a magnetic field can make the material slightly resistive [12] pushing the detector into the latching regime. This prevents relaxation oscillations from being observed, in accordance with the observed detection curve.

The limitation caused by latching is only observed when dark counts are still negligible at comparatively high field strengths. If the temperature is increased,

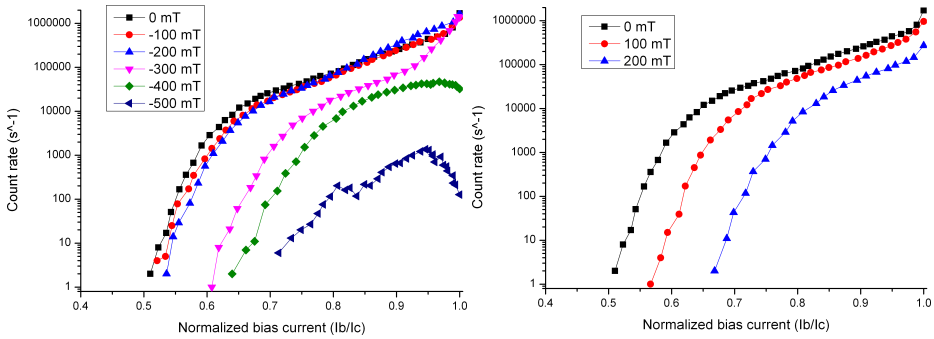

(a) *Light counts as a function of normalized bias current in the negative field direction.*

(b) *Light counts as a function of normalized bias current in the positive field direction.*

Figure 19: *Light counts as a function of bias current normalized to the critical current in a magnetic field perpendicular to the meander in two directions and at 2 K. The negative direction is the direction in which the critical current was shown to increase in section 4.1. The data is the same as that shown in Fig. 17a and Fig. 17b. Rescaling does not collapse the data on a single curve as the hotspot model would predict.*

the critical current decreases and the first mechanism applies in both directions of the field. This can be seen in Fig. 18.

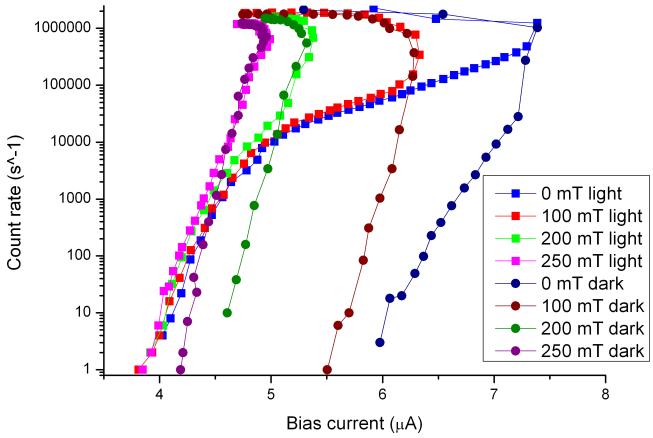

Figure 20: *Detection curves (squares) for a number of different fields in the positive field direction with corresponding dark count curves(circles). For every field strength the dark and light counts overlap at some point and the count rate is dominated by dark counts. As the field is increased, the point where dark counts become dominant is earlier on the detection curve. At 250 mT the current range over which the detector can be used as a photon detector is almost negligible.*

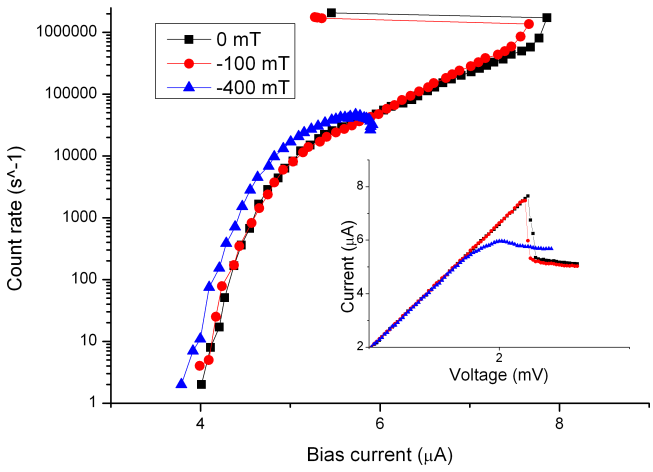

Figure 21: *Detection curves for a number of different fields in the negative field direction. A qualitative change in behavior is observed in the detection curve at -400 mT. Inset: The IV curves corresponding to these detection curves. A qualitative change is also be observed in the IV curve of the device at the same field strength. The IV curve is consistent with latching behavior which may explain the qualitative change in the detection curve.*

5 Conclusion and outlook

Application of a magnetic field perpendicular to the meander plane of an SSPD reveals a number of effects in both the DC behavior of the device, as well as the photon detection behavior. The device was found to behave differently depending on the direction of the magnetic field, indicating an inherent asymmetry present in the detector that is not part of the nominal design. This asymmetry is apparent in the critical current of the device, which was found to be different depending on the direction of the bias current at the same magnetic field. In one direction of the field the critical current was found to be about 8% higher when a magnetic field of 50 mT was applied compared to no field at all.

Dark counts were measured as a function of both bias current and magnetic field strength. Count rates were found to depend on the critical current and were therefore also asymmetric with respect to the direction of the magnetic field. Dark count rates were also found to exhibit local minima when a magnetic field of about 50-100 mT was applied in either direction. At the moment, we are unable to explain these minima. A gradual change from a multiexponential to a monoexponential increase in dark count rate was found to occur for fields lower than 30 mT.

Light detection curves were measured as a function of both bias current, magnetic field strength and temperature. A magnetic field was found to have a very different effect compared to changing the temperature. This can not be explained simply by rescaling with the critical current as the hotspot model would predict. The device was found to function as a photon detector over a range of magnetic field strengths limited either by dark counts or the onset of latching.

The results obtained in this study can not be explained in terms of the critical current as the sole parameter. This means that the effect of a magnetic field can not be accounted for using the hotspot model in its current form. The effect of a magnetic field should probably be explained in terms of vortex dynamics or the Usadel equation [25].

Probing the effect of a magnetic field on the detection process in an SSPD has proven difficult because the field has two different effects that are difficult to separate. First of all, it influences the properties of the bulk material, and secondly, it changes the current distribution in the wire leading to geometric effects. In the future, we hope to resolve this issue by performing experiments on a bow tie shaped constriction nanodetector. Because its geometry is simpler, this device is expected to be less likely to be asymmetric as a result of fabrication errors. In addition, the vortex structure of this geometry is expected to be relatively simple to predict, allowing us to put vortex based fluctuation models to the test.

References

[1] G.N. Goltsman, O. Okunev, G. Chulkova, A. Lipatov, A. Semenov et al. *Picosecond superconducting single-photon optical detector,* Appl. Phys. lett. **79**, 705 (2001)

[2] F. Marsili, V. B. Verma, J. A. Stern, S. Harrington, A. E. Lita, T. Gerrits, I. Vayshenker, B. Baek, M. D. Shaw, R. P. Mirin, and S. W. Nam, *Detecting Single Infrared Photons with 93% System Efficiency,* arXiv:1209.5774 (2012)

[3] Saeedeh Jahanmirinejad, *Superconducting and Photon-Number-Resolving Detectors,* Ph.D. thesis (2012)

[4] M.J. Stevens, B. Baek, E. a. Dauler, A.J. Kerman, R.J. Molnar, S. a. Hamilton, K.K. Berggren, R.P. Mirin, S.W. Nam, *High-order temporal coherences of chaotic and laser light,* Opt. expr.**18**, 1430 (2010)

[5] C. Zinoni, B Alloing, L.H. Li, F. Marsili, A. Fiore, L. Lunghi, A. Gerardino, Y.B. Vakhtomin, K.V. Smirnov, G.N. Goltsman, *Single-photon experiments at telecommunication wavelengths using nanowire superconducting detectors* Appl. Phys. Lett.**91**, 031106 (2007)

[6] M. Halder, A. Beveratos, N. Gisin, V. Scarani, C. Simon, H. Zbinden, *Entangling independent photons by time measurement,* Nat. Phys.**3**, 692 (2010)

[7] R. Hadfield, J. Habif, J. Schlafer, R. Schwall, S. Nam, *Quantum key distribution at 1550 nm with twin superconducting single-photon detectors,* Appl. Phys. Lett. 89, 241129 (2006)

[8] P. Feautrier, E. le Coarer, R. Espiau de Lamaestre, P. Cavalier, L. Maingault, J-C Villagier, L. Frey, J. Claudon, N. Bergeard, M. Tarkhov, J-P Poizat, *High-speed superconducting single photon detectors for innovative astronomical applications ,* Journal of Physics: Conference Series 97, 012087 (2008)

[9] D. M. Boroson, J. J. Scozzafava, D. V. Murphy, B. S. Robinson, *2009 Third IEEE International Conference on Space Mission Challenges for Information Technology,* 23, 9628 (2009).

[10] A. McCarthy, R. J. Collins, N. J. Krichel, V. Fernandez, A. M. Wallace, G. S. Buller, *Long-range time-of-flight scanning sensor based on high-speed time-correlated single-photon counting,* Applied Optics, Vol. 48, Issue 32, pp. 6241-6251 (2009)

[11] A. Engel, A. schilling, K. Il'in and M. Siegel, *Dependence of count rate on magnetic field in superconducting thin-film TaN single-photon detectors,* Phys. Rev. B **86** , 140506(R)(2012)

[12] Micheal Tinkham, *Introduction to superconductivity,* (Mcgraw Hill, 1996)

[13] Jan Zaanen, *The classical condensates,* Lecture notes (1996)

[14] J.J. Renema, G. Frucci, Z. Zhou, F. Mattioli, A. Gaggero, R. Leoni, M.J.A. de Dood, A. Fiore, M.P. van Exter *Nanowire Superconducting Single Photon Detectors are Energy Detectors,* arXiv:1301.3337 (2013)

[15] Jennifer Kitaygorsky, *Photon and Dark Counts in NbN Superconducting Single-Photon Detectors and Nanostripes,* Ph.D. thesis(2008)

[16] M. Hoffherr, D. Rall, K. Ilin, M. Siegel, A. Semenov, H.-W. Hübers and N.A. Gippius *Intrinsic detection efficiency of superconducting nanowire single-photon detectors with different thicknesses,* Appl. Phys. **108**, 014507 (2010)

[17] A.J. Kerman, J.K.W. Yang, R.J. Molnar, E.A. Dauler, K.K. Berggren *Electrothermal feedback in superconducting nanowire single-photon detectors,* Phys. Rev. B **79**, 100509(R) (2009)

[18] A.J. Kerman, E.A. Dauler, W.E. Keicher, J.K.W. Yang, K.K. Berggren, G.N. Goltsman, and B. Voronov *Kinetic-inductance-limited reset time of superconducting nanowire photon counters* Appl. Phys. Lett. **88**, 111116 (2006)

[19] Francesco Marsili, *Single-Photon and Photon-Number-Resolving Detectors Based on Superconducting Nanowires,* Ph.D. thesis (2009)

[20] Jack W. Ekin, *Experimental techniques for low temperature measurements,* (Oxford university press, 2006)

[21] Marc van Kralingen, *Temperature-dependence of NbN photon detector behavior,* Bachelor Thesis (2012)

[22] F. Mattioli, R. Leoni, A. Gaggero, M. G. Castellano, P. Carelli, F. Marsili and A. Fiore, *Electrical characterization of superconducting single-photon detectors,* Appl. Phys. **101** , 054302 (2007)

[23] Sebastien Adam, *Stabilized hotspots and vortex patterns in superconducting NbN and Nb nanostructured strips and loops,* Ph.D. thesis (2011)

[24] *Report on films GaAs 124-2,* TU Eindhoven (2011)

[25] A. Anthore, H. Pothier, D. Esteve, *Density of States in a Superconductor Carrying a Supercurrent,* Phys. Rev. Lett. 90, 127001 (2003)